

Low-pressure clino- to high-pressure clinoenstatite phase transition: A phonon-related mechanism

YONGGANG G. YU^{1,*} AND RENATA M. WENTZCOVITCH^{2,†}

¹Department of Chemistry, Minnesota Supercomputing Institute, University of Minnesota, Minneapolis, Minnesota 55455, U.S.A.

²Department of Chemical Engineering and Materials Sciences, Minnesota Supercomputing Institute, University of Minnesota, Minneapolis, Minnesota 55455, U.S.A.

ABSTRACT

We have investigated by first principles the compressional behavior of low-pressure (LP) and high-pressure (HP) MgSiO₃ clinoenstatite. We have carefully examined unit-cell shapes, chain angles, and polyhedral volume responses, such as angle variances and quasi-elongations, under pressure at room temperature. We have observed opposite behavior of the tetrahedra in the S-rotated and O-rotated chains with pressure in the LP phase, with a slight increase (decrease) in angle variance and quasi-elongation in the former (latter). Inspection of zone center modes of both phases under pressure reveals a transition path that converts the S-rotated chain in the LP phase into the O-rotated chain in the HP phase. This conversion is related to a slight softening of an A_g “metastable” Raman mode under pressure.

Keywords: Phase transition mechanism, low-pressure clinoenstatite, high-pressure clinoenstatite, Raman, IR, phonon frequency

INTRODUCTION

Next to olivine, pyroxenes (which include clinopyroxene and orthopyroxene) are the most abundant constituents of Earth’s upper mantle (Ringwood 1975). It has been suggested (Woodland and Angel 1997; Woodland 1998) that the phase transformation of orthopyroxene to high-pressure clinopyroxene may account for the X-discontinuity at 312 ± 21 km depth observed by Revenaugh and Jordan (1991). The progressive dissolution of pyroxene into garnet increases velocity gradients between depths of 300 and 460 km as pointed out by Ringwood (1967). Natural pyroxenes under pressure are often used as starting materials to produce perovskite at lower mantle conditions in experimental mineral physics.

Because of their abundance in the upper mantle, the polymorphs of the magnesium end-member clinopyroxene, MgSiO₃ clinoenstatite, are among the most investigated minerals under pressure. They exist in the low-pressure *P2₁/c* structure (LP-En hereafter) and high-pressure *C2/c* structure (HP-En hereafter). LP-En exists at ambient conditions, whereas HP-En had eluded unambiguous experimental detection until the 1990s because of its conversion into LP-En structure upon quenching (Angel et al. 1992). In the past few decades, the crystal chemistry, equations of state, and thermodynamic properties of LP- and HP-En have been investigated experimentally by single-crystal or powder X-ray diffraction measurements (Thompson 1970; Krupka et al. 1985; Angel et al. 1992; Angel and Hugh-Jones 1994; Kung et al.

2004; Chopelas 1999; Huang et al. 2000; Lin 2004), molecular dynamics simulations using empirical potentials (Matsui and Price 1992), and by first principles (Wentzcovitch et al. 1995; Duan et al. 2001). However, the transition mechanism for the conversion of LP-En to HP-En has not been addressed so far. Here, we present a comparative study of the compressional behavior of the LP- and HP-En that (1) substantially improves previous density-functional-based zero Kelvin calculations (Wentzcovitch et al. 1995; Duan et al. 2001) and (2) identifies a phonon-related mechanism for the LP-En to HP-En transition.

Both LP-En (*P2₁/c*) and HP-En (*C2/c*) exist in monoclinic structures with the unique axis *b* perpendicular to the other two axes, *a* and *c* (Fig. 1). The obtuse angle, β, between *a* and *c*, is about 107° for LP-En and 103° for HP-En at ambient conditions. What makes pyroxene of special interest is the corner sharing SiO₄ tetrahedral chains running through the crystal along the *c* axis, forming a silicate layer parallel to the *a-c* plane. These SiO₄ tetrahedral chains in LP-En are divided into two types: the “O-rotated” chain (O-chain) and the “S-rotated” chain (S-chain) based on the O₃-O₃-O₃ chain extension angle. This classification characterizes the way these chains are disposed along the *c* direction. LP-En contains both an S-chain and an O-chain with O₃-O₃-O₃ angles of ~205° and ~132°, respectively. To illustrate the transition path mentioned above we choose a counter-clockwise chain extension angle as shown in Figure 1. In HP-En all chains are O-rotated, and the O₃-O₃-O₃ angle is ~134° at ambient conditions. Upon a phase transition from LP-En to HP-En at ~5–8 GPa, the S-chain in LP-En transforms to an O-chain in HP-En. In this paper, we introduce the computational method used in this work. We present a detailed comparison of the compression behavior of LP- and HP-En. Finally, we propose that the LP-En

* Current address: Department of Geosciences, Virginia Polytechnic Institute and State University, Blacksburg, Virginia 24060, U.S.A. E-mail: yonggang@vt.edu

† E-mail: wentzcov@cems.umn.edu

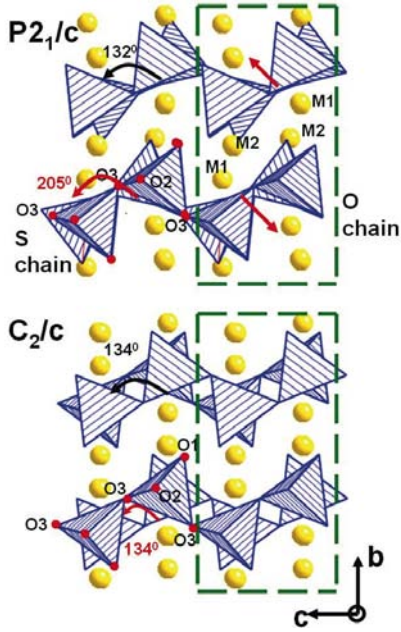


FIGURE 1. Crystal structure of LP-En ($P2_1/c$) and HP-En ($C2/c$) in $MgSiO_3$ at 0 GPa. The O3-O3-O3 angles are defined to be counter-clockwise in convenience for later description of phase transition mechanism. With this definition, O3-O3-O3 angle of S-chain is 205° and that of O-chain is 134° .

to HP-En transition mechanism is related to a slight softening of the lowest Raman mode in LP-En.

COMPUTATIONAL METHOD

We have used density functional theory (DFT) (Hohenberg and Kohn 1964; Kohn and Sham 1965) within the local density approximation (LDA) (Ceperley and Alder 1980) as parametrized by Perdew and Zunger (1981). The pseudopotentials used here have been successfully applied to phase transitions such as perovskite to post-perovskite (Tsuchiya et al. 2004) and the post-spinel dissociation (Yu et al. 2007) in magnesium silicates. The magnesium pseudopotential was generated by the method of von Barth and Car (as described in Dal Corso et al. 1993), which replaces a norm-conserving Mg pseudopotential used by Wentzcovitch et al. (1995) and Duan et al. (2001) to study HP- and LP-En in $MgSiO_3$. The oxygen and silicon pseudopotentials were generated by the method of Troullier and Martins (1991). The plane-wave kinetic energy cutoff (E_{cut}) was chosen to be 80 Ry, and a $4 \times 4 \times 4$ Monkhorst and Pack (1976) k-point mesh with $(\frac{1}{2}, \frac{1}{2}, \frac{1}{2})$ shift from origin was used for Brillouin zone (BZ) samplings of both phases. This ensures the energy convergence with respect to E_{cut} and k-mesh to be within 2.0×10^{-4} Ry/atom. For high-pressure structural relaxations, we have adopted the same variable-cell shape molecular dynamics (VCSMD) method (Wentzcovitch 1991) used in previous DFT studies (Wentzcovitch et al. 1995; Duan et al. 2001). We have calculated Γ -point phonon frequencies using density functional perturbation theory (Baroni et al. 2001). The room-temperature structural parameters reported here were obtained by high-temperature statically constrained quasiharmonic approximation (QHA) (Carrier et al. 2007).

Compressional behavior

Figure 2 shows the pressure dependence of cell parameters of LP- and HP-En from this study at 300 K using statically constrained QHA, from previous static DFT calculations by Duan et al. (2001), and from room-temperature experimental measurements by Angel et al. (1992) and Angel and Hugh-Jones (1994). In fact the ability of the QHA to produce structural parameters has been only recently recognized (Carrier et al. 2007). Compared to the previous LDA results by Duan et al. (2001), the current ones agree considerably better with experimental data. To a great extent, this agreement results from the inclusion of lattice vibrational effects that expand the static lattice parameters. In addition, the magnesium pseudopotential used here is more transferable also. As can be seen, the c axis is substantially stiffer than the a and b axes for both LP- and HP-En. Only a small reduction in the monoclinic angle β with pressure is observed in both phases. Across the LP-En to HP-En transformation at ~ 7 GPa (Angel et al. 1992), abrupt reductions of the a and c axes and of the β angle are observed. This results in a primitive cell-volume reduction from 393.2 to 383.3 \AA^3 and in a density increase of $\sim 2.8\%$. A detailed comparison of LDA calculated unit-cell parameters at 300 K for LP-En (ambient pressure) and HP-En (7.9 GPa) with previous experimental and theoretical studies is shown in Table 1.

To be consistent with a previous study (Wentzcovitch et al. 1995), we have plotted the O3-O3-O3 S-chain angle counted clockwise rather than counter-clockwise in Figure 3. In both LP- and HP-En, we observed a monotonic decrease of the angles in

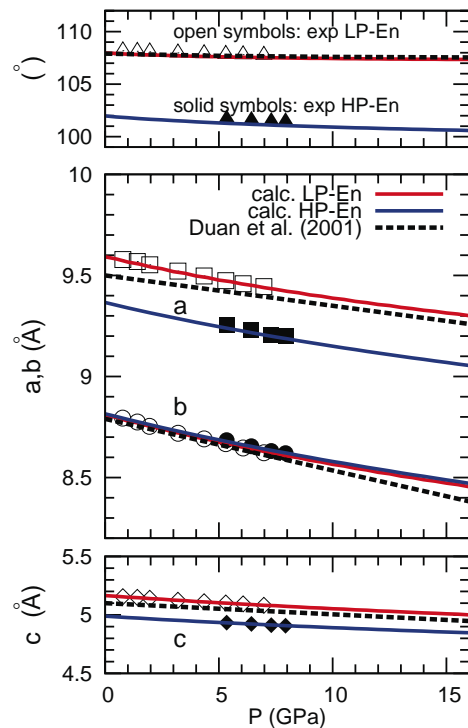


FIGURE 2. Predicted pressure dependence of the lattice parameters of LP- and HP-En at 300 K, compared with experimental measurements (Angel and Hugh-Jones 1994 in symbols) and previous static LDA calculation of LP-En (Duan et al. 2001 in dashed lines).

the O-chains (O3-O3-O3 and Si-O3-Si angles). In LP-En (Fig. 3a), the O₃-O₃-O₃ angle in the S-chain is ~20° larger than that angle in the O-chain at all pressures investigated. For HP-En, we plot the three different bond angles in the O-chain in Figure 3b together with experimental data (Angel et al. 1992) and angles reported by a previous static LDA calculation (Wentzcovitch et al. 1995). Our bond angles at 300 K agree better with experiments than the previous static values by Wentzcovitch et al. (1995) owing to vibrational effects and to the more accurate magnesium pseudopotential (see Dal Corso et al. 1993) used here.

The 300 K polyhedral volumes under pressure are shown in Figure 4. On average, the compressibility, $\beta = -1/V(\partial V/\partial P)T$, of the MgO₆ octahedra is ~2.3× larger than that of SiO₄ tetrahedra. To quantify the degree of polyhedral distortion under compression, we have computed angle variances (AV) and quadratic elongations (QE) (Robinson et al. 1971). AV is defined as the variance of bond angles from their ideal values, i.e., $\sigma_{\text{oct}}^2 = \sum_{i=1,12} (\theta - 90^\circ)^2/11$ for an octahedron and $\sigma_{\text{tet}}^2 = \sum_{i=1,6} (\theta - 109.47^\circ)^2/5$ for a tetrahedron. The angle between bonds, θ , is defined by atoms located at the corner and at the center of these polyhedra. QE is the mean quadratic elongation of the bond lengths (l_i) from those of an ideal polyhedron with the same volume and a single bond length (l_0), i.e., $\lambda_{\text{poly}} = \sum_{i=1,N} (l_i/l_0)^2/N$, with $N = 6$ ($N = 4$) for an

TABLE 1. LDA calculated 300 K unit-cell parameters of MgSiO₃ LP-En (ambient pressure) and HP-En (7.9 GPa) compared with previous experiments and theoretical calculations

	<i>a</i> (Å)	<i>b</i> (Å)	<i>c</i> (Å)	β (°)	<i>V</i> (Å ³ /uc)
LP-En					
this work	9.591	8.809	5.165	107.95	415.2
Ohashi (1984)	9.606	8.8131	5.170	108.35	415.5
Angel and Hugh-Jones (1994)	9.605	8.814	5.169	108.34	415.5
Matsui and Price (1992)	9.600	8.672	5.244	108.60	413.8
Duan et al. (2001)	9.4876	8.6682	5.1050	107.90	399.5
HP-En					
this work	9.186	8.620	4.907	101.0	381.4
Wentzcovitch et al. (1995)	9.12	8.19	4.904	101.3	359.2
Angel et al. (1992)	9.201	8.621	4.908	101.50	381.5

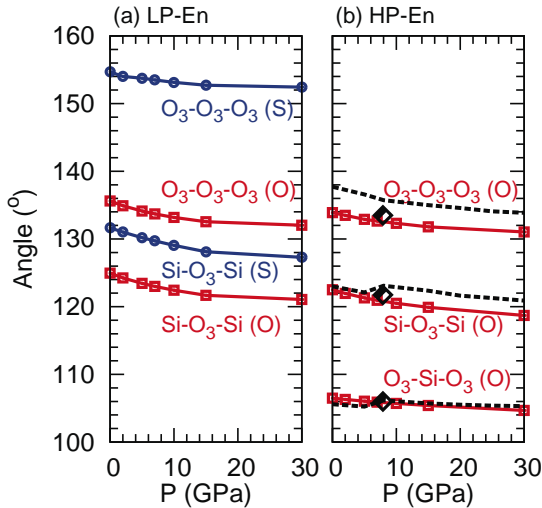


FIGURE 3. Variation of tetrahedral chain angles (see Fig. 1) with pressure. Diamond symbols denote experimental data (Angel et al. 1992) and dashed lines represent previous static calculations (Wentzcovitch et al. 1995).

octahedron (tetrahedron).

Figure 5 displays the calculated AV and QE for polyhedra in LP- and HP-En. Two prominent features appear in LP-En (Fig. 5a). First, among the four types of polyhedra, i.e., M1 and M2 octahedra and S- and O-type tetrahedra, the M2 octahedron is the most distorted. This is indicated by very large AV and QE values of this polyhedron. Second, with increasing pressure, the S-type tetrahedron becomes more distorted, while all other polyhedra become more regular under pressure. This suggests a potential instability of the S-type chain in LP-En. The M2 octahedra in HP-En are much more regular (smaller AV and QE) than the M1 and M2 octahedra in LP-En. Next, we discuss long-wavelength lattice vibrations, that in this case, reveal more than macroscopic compression mechanisms about structural instabilities.

Zone center modes and the transition mechanism

The calculated zone center phonon frequencies of LP- and HP-En are displayed at several (static) pressures and compared with available room-temperature high-pressure experimental Raman and IR data (Chopelas 1999; Huang et al. 2000; Lin 2004)

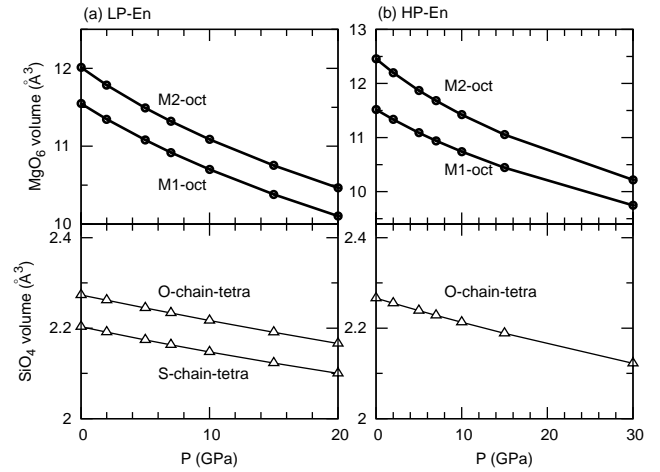


FIGURE 4. Predicted variation of polyhedral volume with pressure at 300 K in LP- and HP-En.

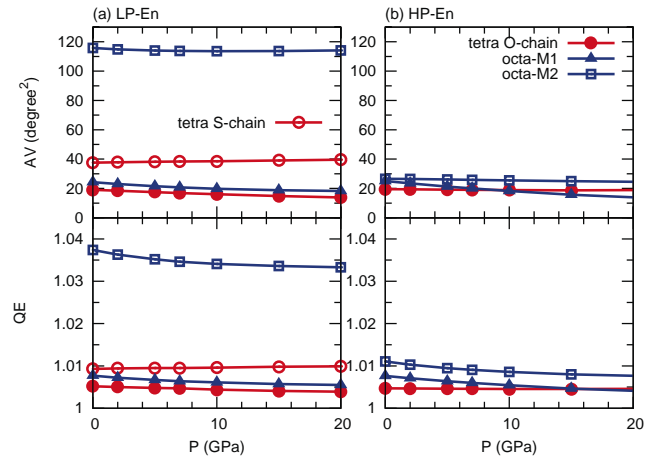


FIGURE 5. Prediction of polyhedral angle variance (AV) and quadratic elongation (QE) as a function of pressure for LP- and HP-En at 300 K.

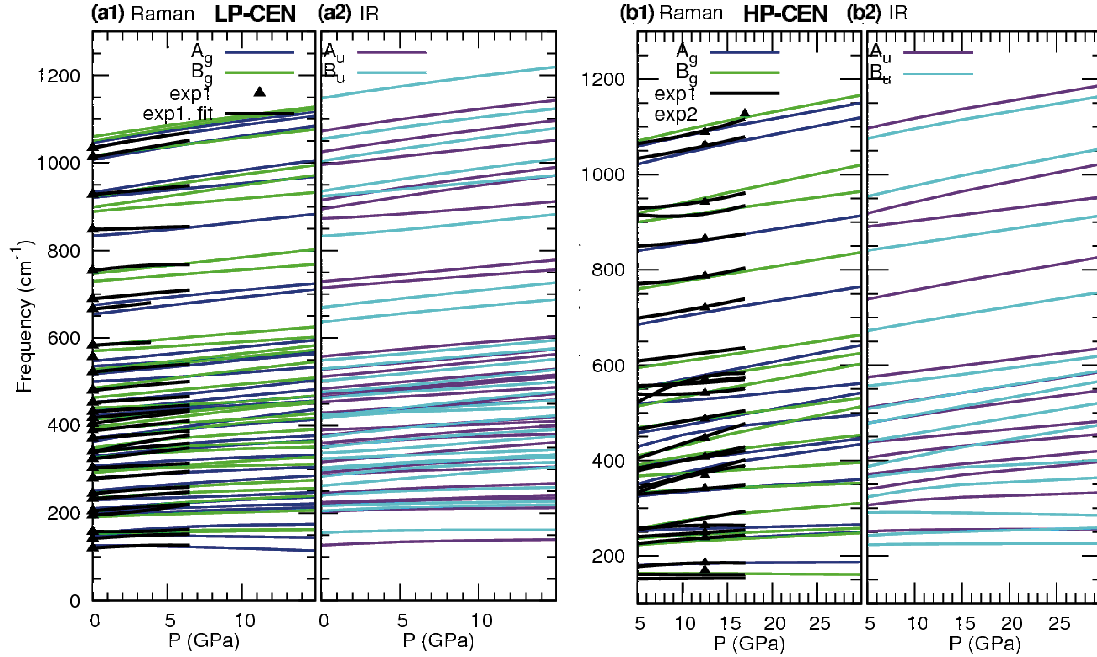


FIGURE 6. Predicted pressure dependence of Raman and IR frequency of LP- and HP-En at 0 K compared to experimental data [exp1 = Lin (2004); exp2 = Chopelas (1999)].

in Figure 6. The colored lines are from this calculation and the black solid lines are Raman frequency vs. pressure fittings at room temperature by Lin (2004). Symbols in Figure 6a are from Raman data at 0 GPa by Lin (2004), while those in Figure 6b are from Raman data at 12.5 GPa by Chopelas and Boehler (1992). They are in very good agreement with our predictions.

An interesting point shown in Figure 6 is that, except for the lowest Raman mode with A_g symmetry, the frequencies of all other modes in LP-En increase with pressure. The softening of the lowest A_g mode with pressure suggests a structural instability related to this mode. Specifically, the phonon frequency of the lowest A_g Raman mode decreases from 125.8 to 124.1 to 119.7 cm^{-1} when pressure is increased from 0 to 5 to 10 GPa, respectively. Note that according to Angel and Hugh-Jones (1994), hysteresis in LP-En ($P2_1/c$) to HP-En ($C2/c$) transition is very large between 5.3 and 7.0 GPa, with the former being the first appearance of $C2/c$ and the latter of $P2_2/c$. The pressures 5.34 and 7.93 refer to decompression and compression transitions, respectively. Closer inspection of the atomic displacements (eigenvector) associated with this mode reveals that it folds the S-chain away from the O-chain and reduces the $\text{O}_3\text{-O}_3\text{-O}_3$ S-chain angle. We investigate the effect of this mode on the structure of LP-En by adding the atomic displacements corresponding to the A_g mode to each atom in the fully relaxed LP-En structure with $P2_1/c$ symmetry at (static) 5 GPa, where cell parameters are 9.287 Å (a), 8.438 Å (b), 4.992 Å (c), and 107.3° (β) (Fig. 7a). We produce an intermediate structure (Fig. 7b) with the same $P2_1/c$ symmetry in which the $\text{O}_3\text{-O}_3\text{-O}_3$ S-chain angle ($\theta_{\text{s-chain}}$ hereafter) is smaller than in the starting configuration ($\sim 207^\circ$). A subsequent relaxation of the entire crystal structure at 5 GPa using VCSMD leads to the $C2/c$ HP-En structure (Fig. 7c), a structure whose space group is a super group of $P2_1/c$. We conclude that the transition path should be along this A_g normal

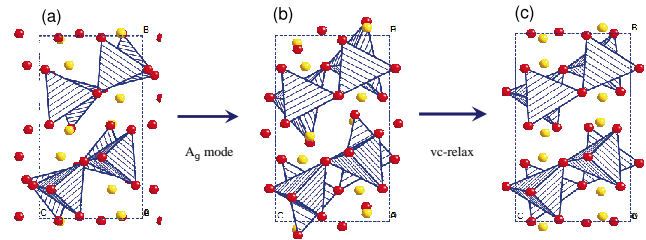


FIGURE 7. (a) $P2_1/c$ LP-En structure at 5 GPa whose cell parameters a , b , c , and β are 9.47, 8.67, 5.1 Å, and 107.6°, respectively; (b) intermediate structure resulting from the superposition of the A_g mode displacement (126 cm^{-1} , see text) to the $P2_1/c$ structure shown in a; (c) $C2/c$ HP-En structure with new cell-parameters a , b , c , and β equal, respectively, to 9.24, 8.68, 4.93 Å, and 101.3° that results from complete structural relaxation at 5 GPa using VCSMD (Wentzcovitch 1991).

mode displacement, because, as we will demonstrate, the effect of this mode is to release the internal pressure (stress) at fixed volume and reduce the enthalpy of the crystal. Here, note that our starting LP-En configuration at 5 GPa is actually unstable relative to the HP-En configuration, because the LDA static transition pressure for the LP-En to HP-En transition is found to be 1.8 GPa.

Plotted in Figure 8 are the dependence of $\theta_{\text{s-chain}}$ on the lowest A_g mode amplitude and of the enthalpy on $\theta_{\text{s-chain}}$ at various monoclinic cell angles β (see caption in Fig. 8). The $P2_1/c$ symmetry, comprising 4 point group operations, is found for all displaced configurations when the A_g mode is applied to LP-En. Meanwhile, the $\theta_{\text{s-chain}}$ decreases monotonically with increasing mode amplitude (at 5 GPa with a fixed cell shape) and the static enthalpy of the crystal decreases to a local minimum at about $\theta_{\text{s-chain}} = 145^\circ$ before it increases again rapidly, irrespective of β . The enthalpy vs. $\theta_{\text{s-chain}}$ curves were generated by varying only

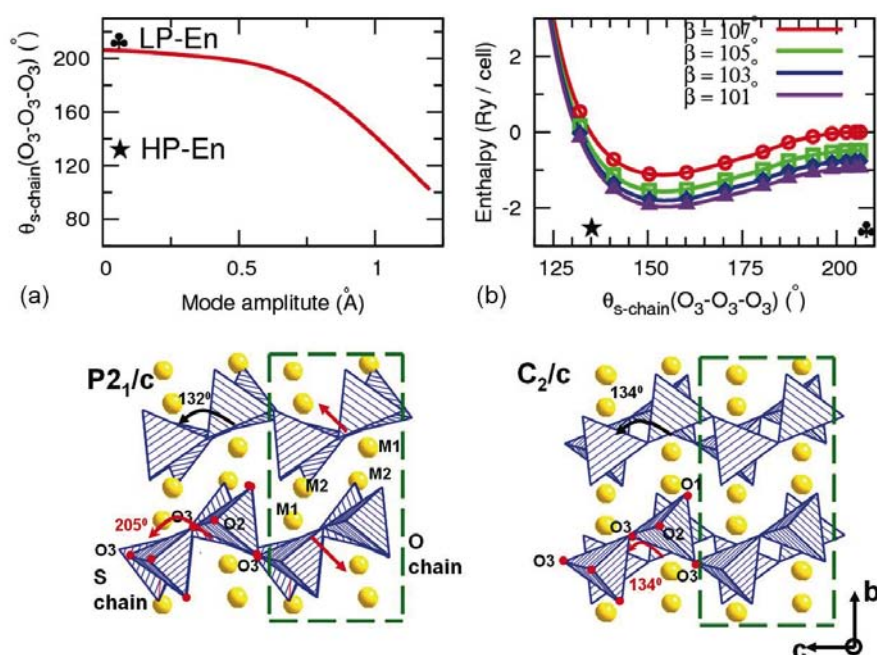


FIGURE 8. (a) Effect of A_g mode displacement amplitude on S-chain rotation angle [$\theta_{s-chain}(O_3-O_3-O_3)$] of LP-En and (b) how this S-chain rotation angle affects the static enthalpy of this structure at various monoclinic cell angles β . Enthalpy is plotted relative to the static enthalpy of fully relaxed LP-En at 5 GPa (static). (There are 40 atoms in one unit cell in LP-En.)

two degrees of freedom in the structure equilibrated at 5 GPa: $\theta_{s-chain}$, through the application of the A_g mode displacement, and β , the monoclinic cell angle. No structural relaxation was performed at this point. This plot indicates that, indeed, the displacement of atoms according to the A_g mode decreases the enthalpy at 5 GPa. This is because along this path where the $\theta_{s-chain}$ varies from $\sim 205^\circ$ to $\sim 145^\circ$ to $\sim 125^\circ$ with increasing mode amplitude at $\beta = 107^\circ$, the internal pressure decreases from the initial pressure, 5 GPa, to 4 GPa, where enthalpy is lowest, and then increases again. A similar trend was observed at other fixed β angles. The consequence is a dramatic decrease then a rapid increase in static enthalpy with increasing A_g mode amplitude (or with decreasing $\theta_{s-chain}$). Therefore this appears to be a viable path for the LP-En to HP-En transition. As mentioned above, structural relaxation after application of this mode to LP-En at 5 GPa leads to the HP-En structure. This is not a soft mode transition and the A_g mode frequency decreases only slightly before the transition takes place. Instead, the chain rotation leading LP-En to HP-En is a discontinuous, first order, enthalpically driven event that could take place along the path provided by the A_g displacement mode. Other paths are not ruled out at this point, but the current result strongly suggests that the transformation mechanism is related with this phonon mode.

ACKNOWLEDGMENTS

This research was supported by NSF grants: Earth-0230319, Earth-0635990, and ATM-0428774. Computations were performed at the Minnesota Supercomputing Institute.

REFERENCES CITED

- Angel, R.J. and Hugh-Jones, D.A. (1994) Equations of state and thermodynamic properties of enstatite pyroxenes. *Journal of Geophysical Research*, 99, 19777–19783.
- Angel, R.J., Chopelas, A., and Ross, N.L. (1992) Stability of high-density clinoenstatite at upper-mantle pressures. *Nature*, 358, 322–324.
- Baroni, S., de Gironcoli, S., Corso, A.D., and Giannozzi, P. (2001) Phonons and related crystal properties from densityfunctional perturbation theory. *Reviews of Modern Physics*, 73, 515–562.
- Carrier, P., Wentzcovitch, R., and Tsuchiya, J. (2007) First-principles prediction of crystal structures at high temperatures using the quasiharmonic approximation. *Physical Review B*, 76, 064116.
- Ceperley, D.M. and Alder, B.J. (1980) Ground state of the electron gas by a stochastic method. *Physical Review Letters*, 45, 566–569.
- Chopelas, A. (1999) Estimates of mantle relevant Clapeyron slopes in the $MgSiO_3$ system from high-pressure spectroscopic data. *American Mineralogist*, 84, 233–244.
- Chopelas, A. and Boehler, R. (1992) Raman spectroscopy of high pressure $MgSiO_3$ phases synthesized in a CO_2 laser heated diamond anvil cell: Perovskite and clinopyroxene. In Y. Syono and M. Manghni, Eds., *High-Pressure Research: Application to Earth and Planetary Sciences*, p. 101–108. Terra Scientific Publications Co., Tokyo.
- Dal Corso, A., Baroni, S., Resta, R., and de Gironcoli, S. (1993) Ab initio calculation of phonon dispersions in II-VI semiconductors. *Physical Review B*, 47, 3588–3592.
- Duan, W.H., Karki, B.B., Wentzcovitch, R.M., and Gu, B.L. (2001) Ab initio study of $MgSiO_3$ low-clinoenstatite at high pressure. *American Mineralogist*, 86, 762–766.
- Hohenberg, P. and Kohn, W. (1964) Inhomogeneous electron gas. *Physical Review*, 136, 864–871.
- Huang, E., Chen, C.H., Huang, T., Lin, E.H., and Xu, J. (2000) Raman spectroscopic characteristics of Mg-Fe-Ca pyroxenes. *American Mineralogist*, 85, 473–479.
- Kohn, W. and Sham, L.J. (1965) Self-consistent equations including exchange and correlation effects. *Physical Review*, 140, 1133–1138.
- Krupka, K.M., Hemingway, B.S., Robie, R.A., and Kerrick, D.M. (1985) High-temperature heat capacities and derived thermodynamic properties of anthophyllite, diopside, enstatite, dolomite, bronzite, talc, tremolite, and wollastonite. *American Mineralogist*, 70, 261–271.
- Kung, J., Li, B., Uchida, T., Wang, Y., Neuville, D., and Liebermann, R.C. (2004) In situ measurements of sound velocities and densities across the orthopyroxene \rightarrow high-pressure clinopyroxene transition in $MgSiO_3$ at high pressure. *Physics of the Earth and Planetary Interiors*, 147, 27–44.
- Lin, C.-C. (2004) Pressure-induced polymorphism in enstatite ($MgSiO_3$) at room temperature: Clinoenstatite and orthoenstatite. *Journal of Physics and Chemistry of Solids*, 65, 913–921.
- Matsui, M. and Price, G.D. (1992) Computer simulation of the $MgSiO_3$ polymorphs. *Physics and Chemistry of Minerals*, 18, 365–372.
- Monkhorst, H.J. and Pack, J.D. (1976) Special points for Brillouin-zone integrations. *Physical Review B*, 13, 5188–5192.
- Ohashi, Y. (1984) Polysynthetically-twinning structures of enstatite and wollastonite. *Physics and Chemistry of Minerals*, 10, 217–229.
- Perdew, J. and Zunger, A. (1981) Self-interaction correction to density-functional approximations for many-electron systems. *Physical Review B*, 23, 5048–5079.
- Revenaugh, J. and Jordan, T.H. (1991) Mantle layering from ScS reverberations. 2. The transition zone. *Journal of Geophysical Research*, 96, 19763–19780.

- Ringwood, A.E. (1967) The pyroxene-garnet transformation in the Earth's mantle. *Earth and Planetary Science Letters*, 2, 255–263.
- (1975) *Composition and Petrology of the Earth's Mantle*, Ch. 14-3. McGraw-Hill, New York.
- Robinson, K., Gibbs, G.V., and Ribbe, P.H. (1971) Quadratic elongation: A quantitative measure of distortion in coordination polyhedra. *Science*, 172, 567–570.
- Thompson, J.B. (1970) Geometric possibilities of amphibole structures and biopyroxenes. *American Mineralogist*, 55, 292–293.
- Troullier, N. and Martins, J.L. (1991) Efficient pseudopotentials for plane-wave calculations. *Physical Review B*, 43, 1993.
- Tsuchiya, T., Tsuchiya, J., Umemoto, K., and Wentzcovitch, R.M. (2004) Phase transition in MgSiO₃ perovskite in the Earth's lower mantle. *Earth and Planetary Science Letters*, 224, 241–248.
- Wentzcovitch, R.M. (1991) Invariant molecular-dynamics approach to structural phase transitions. *Physical Review B*, 44, 2358–2361.
- Wentzcovitch, R.M., Hugh-Jones, D.A., Angel, R.J., and Price, G.D. (1995) Ab-initio study of MgSiO₃ C2/c enstatite. *Physics and Chemistry of Minerals*, 22, 453–460.
- Woodland, A.B. (1998) The orthorhombic to high-*P* monoclinic phase transition in Mg-Fe pyroxenes: Can it produce a seismic discontinuity? *Geophysical Research Letters*, 25, 1241–1244.
- Woodland, A. and Angel, R. (1997) Reversal of the orthoferrosilite-high-*P* clinofersilite transition; a phase diagram for FeSiO₃ and implications for the mineralogy of the Earth's upper mantle. *European Journal of Mineralogy*, 9, 245–254.
- Yu, Y.G., Wentzcovitch, R.M., Tsuchiya, T., Umemoto, K., and Weidner, D.J. (2007) First principles investigation of the postspinel transition in Mg₂SiO₄. *Geophysical Research Letters*, 34, 10306.

MANUSCRIPT RECEIVED AUGUST 8, 2008

MANUSCRIPT ACCEPTED DECEMBER 10, 2008

MANUSCRIPT HANDLED BY GUOYIN SHEN